ISSN 1288-1619

CNRS - Université Pierre et Marie Curie - Université Versailles-Saint-Quentin
CEA - ORSTOM - Ecole Normale Supérieure - Ecole Polytechnique

Institut Pierre Simon Laplace
des Sciences de l'Environnement Global

Notes du Pôle de Modélisation

RiTHM (River Transfer Hydrological Model) : a Runoff Routing Scheme for GCMs

Agnès Ducharne (1,4), Catherine Golaz (2,5), Etienne Leblois (3), Katia Laval (1), Emmanuel Ledoux (2), and Ghislain de Marsily (4)

(1) IPSL - Laboratoire de Météorologie Dynamique, Université Pierre et Marie Curie, Paris, France
(2) Laboratoire Sisyphe, Centre d Informatique Géologique, ENSMP, Fontainebleau, France
(3) Cemagref, Lyon, France
(4) Laboratoire Sisyphe, Université Pierre et Marie Curie, Paris, France
(5) BRGM, Orléans, France

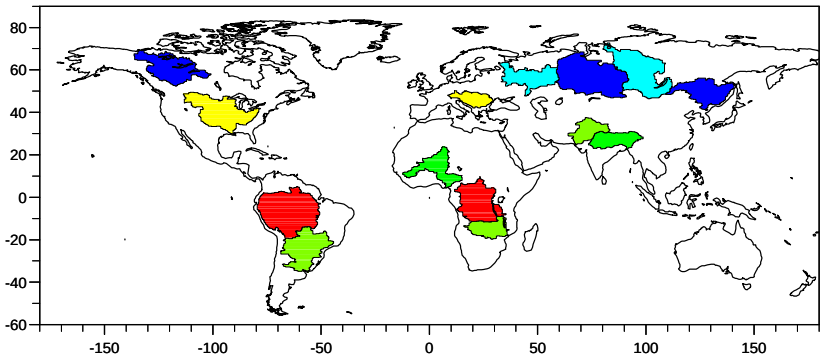

Février 2001 **Note n° 20**

CNRS - Université Pierre et Marie Curie - Université Versailles-Saint-Quentin
CEA -CNES - ORSTOM - Ecole Normale Supérieure - Ecole Polytechnique

I P S L

Institut Pierre Simon Laplace
des Sciences de l'Environnement Global

CETP - LMD - LODYC - LPCM - LSCE - SA

Université Pierre-et-Marie-Curie
B 102 - T15-E5 - 4, Place Jussieu
75252 Paris Cedex 05 (France)
Tél : (33) 01 44 27 39 83
Fax : (33) 01 44 27 37 76

Université Versailles-Saint-Quentin
23 rue du Refuge
78035 Versailles Cedex (France)
Tél : (33) 01 39 25 58 23
Fax : (33) 01 39 25 58 18

Large-scale runoff routing models are important as a validation tool for GCMs, and to close the hydrological cycle in fully-coupled climate models. RiTHM (River-Transfer Hydrological Model) was developed to simulate the discharge of large rivers from the total runoff simulated by the LMD GCM. This conceptual model is discretized on a 1024×800 grid (mean resolution of 25×25 km^2), nested in the 64×50 grid of the LMD GCM. The runoff simulated in a GCM grid cell is uniformly distributed over the 256 nested cells, where a series of two reservoirs accounts for the delay related to water flow through the unsaturated zone and aquifers. The resulting river runoff is then transported assuming pure translation along the drainage network, extracted with a GIS from a 5-minute digital elevation model. The transfer time from a cell to the outlet depends on the lengths and slopes of the downstream cells, and on the basin concentration time. This parameter, which defines the highest transfer time to the outlet in the basin, is the most effective parameter in RiTHM, and we show how it can be related to known topographic and hydrologic characteristics of a basin. We also compare the simulated and observed discharges in selected large river basins representative of major hydroclimatological regimes: RiTHM allows a good phasing of the simulated discharge compared to observations, but the simulated volumes are not realistic, which is mainly related to biases in the GCM's precipitation rates. Yet, neglecting processes such as soil freezing or direct evaporation from the river bed may be another important error source for the simulated discharge, as highlighted by case studies of the Yenisei and Niger basins.

Février 2001 , Note n° 20

Directeur de publication : Jean Jouzel, Directeur de l'IPSL
ISSN 1288-1619

RiTHM (River Transfer Hydrological Model) : a Runoff Routing Scheme for GCMs

Agnès Ducharne[1,4], Catherine Golaz[2,5], Etienne Leblois[3],
Katia Laval[1], Emmanuel Ledoux[2] and Ghislain de Marsily[4]

[1] Laboratoire de Météorologie Dynamique, Université Pierre et Marie Curie, Paris, France

[2] Laboratoire Sisyphe, Centre d'Informatique Géologique, ENSMP, Fontainebleau, France

[3] Cemagref, Lyon, France

[4] Laboratoire Sisyphe, Université Pierre et Marie Curie, Paris, France

[5] Presently at BRGM, Orléans, France

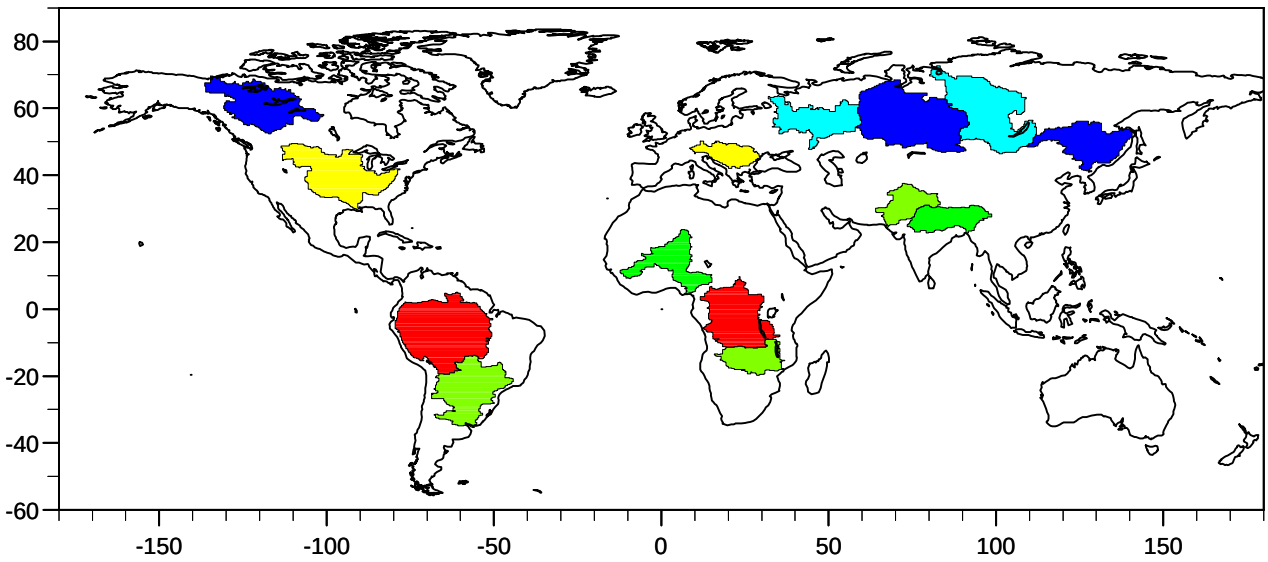

Corresponding address:
Agnès Ducharne
UMR Sisyphe; UPMC Boite 123; 4 place Jussieu; 75252 Paris cedex 05; France
Tel: 33.1.44.27.51.27 Fax: 33.1.44.27.51.25
e-mail: ducharne@biogeodis.jussieu.fr

Abstract

Large-scale runoff routing models are important as a validation tool for GCMs, and to close the hydrological cycle in fully-coupled climate models. RiTHM (River-Transfer Hydrological Model) was developed to simulate the discharge of large rivers from the total runoff simulated by the LMD GCM. This conceptual model is discretized on a 1024×800 grid (mean resolution of 25×25 km^2), nested in the 64×50 grid of the LMD GCM. The runoff simulated in a GCM grid cell is uniformly distributed over the 256 nested cells, where a series of two reservoirs accounts for the delay related to water flow through the unsaturated zone and aquifers. The resulting river runoff is then transported assuming pure translation along the drainage network, extracted with a GIS from a 5-minute digital elevation model. The transfer time from a cell to the outlet depends on the lengths and slopes of the downstream cells, and on the basin concentration time. This parameter, which defines the highest transfer time to the outlet in the basin, is the most effective parameter in RiTHM, and we show how it can be related to known topographic and hydrologic characteristics of a basin. We also compare the simulated and observed discharges in selected large river basins representative of major hydroclimatological regimes: RiTHM allows a good phasing of the simulated discharge compared to observations, but the simulated volumes are not realistic, which is mainly related to biases in the GCM's precipitation rates. Yet, neglecting processes such as soil freezing or direct evaporation from the river bed may be another important error source for the simulated discharge, as highlighted by case studies of the Yenisei and Niger basins.

Keywords: River basins, Runoff routing, Discharge, GCMs, Land surface processes

1 Introduction

The last decade has seen the development of many runoff routing schemes for general circulation models (GCMs). The main motivation behind this work is that runoff, as simulated by GCMs, is a local flux, given per unit surface. It is therefore fundamentally different from riverflow, which is yet needed for several purposes in the field of climate studies. First, riverflow is useful for the validation of land-surface parameterizations, owing to the numerous measurements of riverflow, that integrates land-hydrology (and its response to land energy budget) at a large spatial scale, which is consistent with the GCM scale. Since riverflow can have very long time series, like the 106-year record of the Volga discharge at Volgograd, available from the Global Runoff Data Center (GRDC, Koblenz, Germany), it also allows a validation of the long-term variability of the simulated climate.

Second, riverflow is required to close the global water cycling through oceans, atmosphere and land, and it should therefore not be neglected in coupled ocean/atmosphere GCMs. This fact is supported by many recent studies suggesting a wide spectrum of interactions between rivers and the climate system. An important consequence of fresh water input to the oceans is the creation of a barrier layer around some river mouths, which enhances a local increase of sea surface temperature by preventing the mixing of surface and deep waters. This may influence convection, as shown by Murtuggudde (1998) in the tropical Atlantic, and by Weller (1998) in the Gulf of Bengal for the special case of the summer Indian monsoon. Mysak et al. (1990) suggest that variations of river discharge in the Arctic ocean alter its salinity and circulation, and therefore sea-ice transport through the Fram strait. Also, Campos et al. (1999) suggest that discharge from the Rio de la Plata (Argentina) could be a link between ENSO (El Niño-Southern Oscillation) and the interannual variability of coastal currents along the Atlantic coast of South America (South Brazil Bight).

There are many different runoff routing models (RRM) for large-scale river basins, and most of them, especially among those used in GCMs, belong to the "linear-reservoir" RRMs. In such models, the grid-cells are linear reservoirs (characterized by a transfer coefficient, in time^{-1}), discharging into one another along the drainage network. As reviewed by Arora and Boer (1999), the transfer coefficients, also related to velocities given the length of cells, can be: (1) constant over time and space (e.g. Oki et al., 1999), (2) constant in time but spatially dependent on topography (Miller et al., 1994; Hagemann and Dümenil, 1998) and/or mean discharge (Liston et al., 1994; Vörösmarty et al., 1989), or (3) variable in both space and time, as a function of topography, channel characteristics and discharge, using Manning's equation (Arora and Boer, 1999). A common feature of these linear-reservoir RRMs is a rather coarse resolution, usually ranging from $5^\circ \times 4^\circ$ (mean cell area $\simeq$ 160 000km^2; e.g. Liston et al., 1994; Miller et al., 1994) to $0.5^\circ \times 0.5^\circ$ (mean cell area $\simeq$ 2000km^2; Vörösmarty et al., 1989; Hagemann and Dümenil, 1998). This may distort the influence of topography on transfer times. The only higher resolution RRMs known to the authors are the models SWAM (Coe, 1998) and its descendant HYDRA (Coe, 2000), working at the 5'$\times$5' resolution ($\simeq$ 10 km $\times$ 10 km at the equator).

This paper presents a new RRM, developed with special emphasis on high spatial resolution. This model, RiTHM (for River-Transfer Hydrological Model), is based on the hydrological model MODCOU

(Ledoux, 1980; Ledoux et al., 1989). The latter is a spatially-distributed model, which jointly describes surface and groundwater flow at the daily timestep. First, in every surface cell, surface runoff and deep infiltration are calculated from precipitation and potential evapotranspiration using a conceptual reservoir-based approach. Surface runoff is transferred through the drainage network with transfer times that depend on topography (length and slope of the downstream cells) and a basin-wide parameter, the concentration time. Infiltration, on the other hand, is added to groundwater (which can consist of multi-layered aquifers). It can previously be delayed through the unsaturated zone using a cascade of equal linear reservoirs (Nash, 1959). This infiltration flow contributes to the dynamics of groundwater, given in each aquifer by a finite-difference solution of the two-dimensional diffusivity equation. The resulting head is dynamically coupled to the water level in surface "river" cells, and therefore contributes to riverflow.

The above MODCOU model has been successfully applied at different scales. French examples include, among others: the watersheds of the Haute-Lys (85 km^2) and the Caramy (250 km^2) (Ledoux, 1980); the watershed of the Fecht river (450 km^2) in the Vosges mountains (Ambroise et al., 1995); the HAPEX-MOBILHY study area of more than 14500 km^2 in South-West France (Boukerma, 1987). MODCOU has also been tested in the French part of the Rhône river, with a contributing area of 87000 km^2 (Golaz, 1999; Habets et al., 1999). The last ongoing application of MODCOU (Gomez et al., 1999) involves the Seine river in the framework of the Piren-Seine research programme, devoted to the hydroecology of the Seine river basin ($\simeq$ 75000 km^2). In such context, RiTHM can be seen as an adaptation of the hydrological model MODCOU to the macro-scale, for application to the largest river basins in the world.

The modeling strategy is described in section 2, and section 3 presents the application of RiTHM to 15 macro-scale river basins. Section 4 evaluates the skill of this model to transform the runoff simulated in the GCM of the Laboratoire de Météorologie Dynamique (LMD) into riverflow in these 15 basins. It also presents interesting results showing the need to incorporate new processes in the models describing land hydrology in GCMs. Finally, in section 5, the approach underlying RiTHM is summarized, and its limits are discussed.

2 Model description

2.1 Modeling Strategy

Figure 1 illustrates the overall strategy to simulate riverflow using RiTHM, given boundary conditions comprising runoff on one the hand and topography on the other hand.

RiTHM has been developed to be easily forced by the runoff simulated by the land-surface scheme of the LMD GCM (section 2.2). The main features of this atmospheric GCM are described in Sadourny and Laval (1984) and Le Treut and Li (1991). It is a finite-difference, primitive equation model, that uses a standard sigma-coordinate in the vertical. In the horizontal, the grid-points are distributed regularly in longitude and sine of latitude, defining grid-cells of equal area across the globe. For this study, we used 11 vertical levels and 64$\times$50 grid-points in the horizontal, resulting in grid-cells of approximately 160,000 km^2

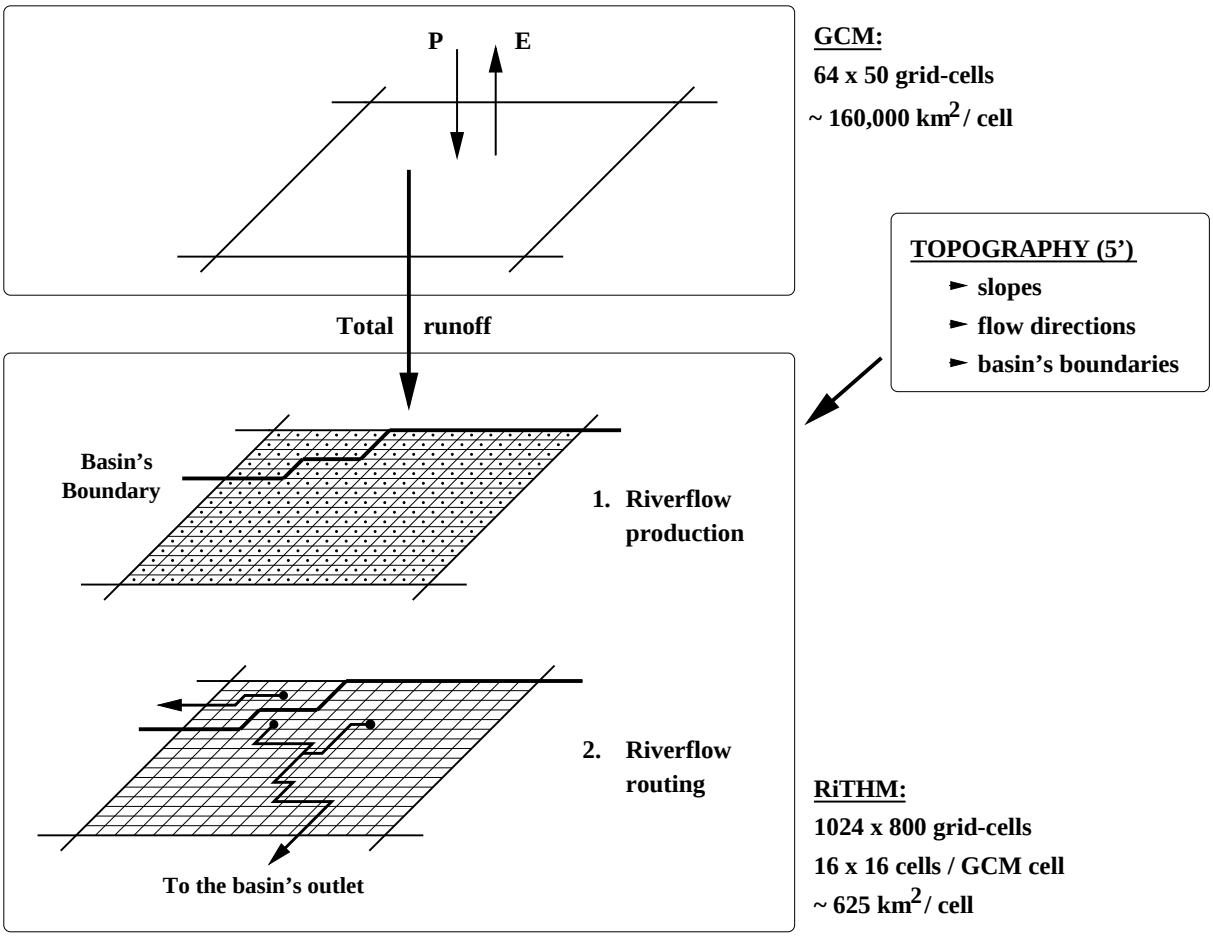

Figure 1: *Overall strategy to simulate riverflow in the LMD GCM using RiTHM.*

and a resolution in the tropics of about $5.6° \times 2.4°$.

The resolution of RiTHM is much finer than that of the GCM, since every GCM grid-cell is subdivided into 16×16 cells. Like in the GCM, the grid-points are distributed regularly in longitude and sine of latitude, and all the grid-cells in RiTHM have the same area of about 625 km^2. Total runoff (surface runoff + baseflow) simulated in a GCM cell is uniformly distributed over the 256 underlying RiTHM cells, where a "riverflow production" module transforms runoff over the RiTHM cell into riverflow at the outlet of this RiTHM cell (section 2.5).

Then, a "riverflow routing" module (section 2.4) performs the downstream transfer of the riverflow from each RiTHM cell to the outlet of the river basin, at the daily time step. This routing is a function of topography, which was derived at RiTHM's resolution from a 5-minute resolution digital elevation model (DEM). Based on this topography, one can characterize the slope of a grid-cell, then the dominant flow direction from each cell (among four directions: north, east, south and west), and therefore delineate the boundaries of the river basins and characterize their drainage network (section 2.3).

2.2 Runoff production in the LMD GCM

Runoff in the LMD GCM is calculated at the 30-minute timestep by the land-surface scheme SECHIBA (Ducoudré et al., 1993). This model represents vegetation owing to the "mosaic" strategy (Avissar and Pielke, 1989; Koster and Suarez, 1992): the heterogeneous vegetation cover of a GCM grid-cell is described by a set of homogeneous "tiles", each tile representing a different land surface type (bare soil or one among seven vegetation types). The total evaporation is computed as the weighted average of the contributions from all the tiles in a grid-cell. The modeled evaporative fluxes from each tile are: interception loss (evaporation of the water intercepted by the canopy), snow sublimation, bare soil evaporation and transpiration, controlled by resistances increasing with environmental stresses (dry soil, dry air, high insolation).

Water can be stored in the canopy interception reservoir, a 1-layer snowpack and a 2-layer soil reservoir. The original functioning of the latter is based on Choisnel's ideas (Ducoudré et al., 1993; Choisnel et al., 1995) and described in details in Ducharne and Laval (2000). The depth of active soil is one meter and the water-holding capacity is globally equal to 150 $kg.m^{-2}$ (except in deserts where it is set at 30 $kg.m^{-2}$). The described soil hydrological processes are the partitioning between surface runoff and infiltration, the diffusion between the two soil layers, and baseflow. The parameterization of surface runoff relies on a statistical-dynamical description of the small-scale variability of soil, known as the Arno (Dümenil and Todini, 1992; Rowntree and Lean, 1994) or VIC (Wood et al., 1992; Liang et al., 1994) approach. It introduces a subgrid-scale distribution of local storage capacity, with local capacities smaller than 150 $kg.m^{-2}$ that can reach saturation and give rise to runoff before the saturation of the whole grid-cell.

The snow processes, and their influence on runoff, are very simple in SECHIBA. The 1-layer snowpack is represented by one water-equivalent prognostic variable, expressed in mm of water. This term is increased by snow fall (the form of precipitation when air temperature is below freezing) and decreased by snow sublimation and snow melt (all three terms in mm of water). Snow melt occurs when the surface

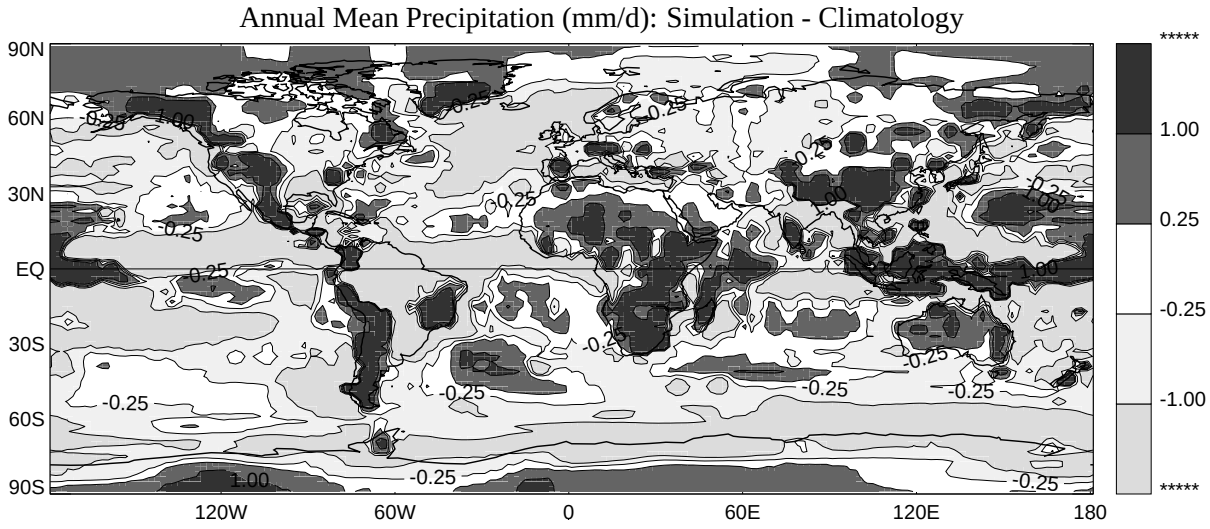

Figure 2: *Precipitation difference (in mm/d) between the mean annual field simulated by the LMD GCM over 1980-1988 and the annual climatology of Legates and Willmott (1990). The positive/negative differences appear in dark/light gray.*

temperature of a cell is above freezing, at the rate which insures that the surface temperature (here the snow temperature) does not exceed 273.15 K. The resulting water flux comprises with throughfall the water that is partitioned between surface runoff and infiltration. The corresponding energy flux is considered in the surface energy budget and influences the surface temperature of the cell.

Runoff in the present application comes from a former simulation of the LMD GCM coupled to the above version of the land-surface scheme SECHIBA (simulation "TOT" of Ducharne et al. (1998)). In this simulation, the LMD GCM is forced with 10 years (1979-1988) of interannually varying sea surface temperatures (SST) from the AMIP dataset (Gates, 1992). This simulation shows a large overestimation of mean precipitation over land (1021 mm/y) compared to the available climatologies. For instance, Legates and Willmott (1990) provide an estimate of 820 mm/yr for gauge-corrected precipitation over land. This overestimation of mean precipitation over land (large enough to be significant despite disparities in the time period of the simulation and the climatologies) is related to a systematic overestimation of continental evaporation (518 mm/y) and total runoff (503 mm/y). Beyond global water budgets, Figure 2 shows the main weaknesses of the simulation used in this study in terms of spatial patterns. The overestimation of precipitation is especially strong over the mountainous areas (where it is persistent most of the year) and in the Inter-Tropical Convergence Zone. The regional underestimations of precipitation are usually weaker, and one reason is that they are seasonal for a large part. This is the case in Amazon basin, where the simulated precipitation is the lowest during the rainy season, and in the northern hemisphere rainbelts (Europe and eastern North-America), where it is too low in summer, but overestimated in winter, although to a lesser extent. A more detailed analysis of this simulation can be found in Ducharne et al. (1998).

2.3 Drainage Network

Topography was interpolated to RiTHM's resolution from the 5-minute resolution DEM ETOPO5 (NGDC, 1988). This resolution is consistent with the recommendations of Maidment (1996) to construct a global drainage network. The slopes dz/dx et dz/dy along the meridian and zonal directions were computed from the average elevation of each cell, using a third-order finite-difference method (Leblois and Sauquet, 2000; Cavazzi, 1995). The final slope was then given by

$$\tan\beta = \sqrt{(dz/dx)^2 + (dz/dy)^2} \tag{1}$$

and the flow direction by

$$\tan(\text{direction}) = \frac{dz/dx}{dz/dy} \tag{2}$$

In each cell, the latter was finally binned into one of four directions classes: north, east, south, and west. For example, the direction class "east" comprises all directions in $]-\pi/4, \pi/4]$. The definition of a unique flow direction from each cell forbids the representation of divergent flows typical of deltas. The reciprocal advantage is to prevent circular flow, which more than counterbalances the approximation of deltas by single streams.

At this point, other problems arose from using a mean elevation in every grid-cell: one problem is the existence of "pits" (when the 4 possible neighbours of a cell have higher elevation, which interrupts the drainage network), and another occurs in flat zones, where no flow direction can be defined from elevation only. A standard pit-removal algorithm (looking for a lower-elevation cell in a distance of three cells from the pit) allowed us to eliminate most artificial pits, but ensured that large natural depressions were retained. Different methods have been proposed to further correct numerical drainage networks from the flat areas and remaining pits. One method is "stream burning" (Maidment, 1996; Renssen and Knoop, 2000): the location of the main streams, derived from maps or available datasets, is digitalized at the resolution of the drainage network, and this information is used to alter the mean elevation in the problem areas. We chose rather to perform corrections on flow directions, which were manually forced to mimic maps of the hydrographic network. This strategy is similar to the one used by Oki and Sud (1998). Where flow direction was modified, the original slope was kept, except of course in flat areas. There, a minimum slope $\tan\beta_0$ was imposed. We imposed a minimum elevation difference of 0.5 m between two connected cells in a flat area, which leads on average to the minimum slope $\tan\beta_0$=2.10^{-5}. Another possible problem, related to resolution, is the artificial capture of one stream by another when the two streams happen in reality to flow in the same cell. This problem is also corrected manually, by forcing the two streams to flow in adjacent cells.

The corrected flow directions allowed us to recursively characterize the entire drainage network and delineate the boundaries of the river basins. Figure 3 compares the resulting areas of 15 major river basins (shown in Figure 8) to their area estimated at the GCM resolution from a manual delineation (a GCM grid-cell being included either entirely or not at all in a river basin). These calculated areas are also compared to a reference value, which is the mean area of several published sources (Renssen and Knoop, 2000). This figure first shows the excellent accuracy of the river basins areas in RiTHM. It also reveals a logical gain in

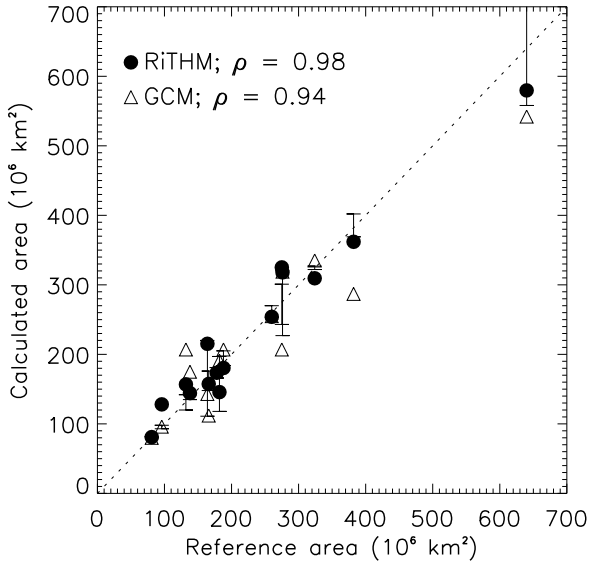

Figure 3: *Comparison in 15 large-scale river basins of the calculated area (at the resolution of RiTHM and the GCM) vs. a reference area. The latter is the mean area of several published sources and the error bars indicate the minimum and maximum areas among these sources (Renssen and Knoop, 2000).*

accuracy when the resolution increases from the GCM to RiTHM, due to a better definition of the basins boundaries.

2.4 Riverflow Routing

The main simplification of RiTHM compared to the hydrological model MODCOU is based on the assumption that, in any 625 km^2 grid-cell, there is at least one stream hydraulically connected to the water table. As a result, the water that infiltrates to the aquifer in a grid-cell — and is later transferred laterally in this aquifer — shall be drained by a stream in the same grid-cell where the initial infiltration took place. This hypothesis assumes that the groundwater flow through deep confined aquifer system is low in comparison to the flow through the phreatic one. This legitimate assumption brings a lot of convenience to the model because it allowed us to discard all physical parameterizations related to groundwater: vertical infiltration through the vadose (unsaturated) zone, groundwater flow and interactions between rivers and water tables. In this simplified framework, the lag related to these processes is accounted for by one infiltration reservoir (section 2.5). An important advantage of this simplification, beyond the spare of CPU, is to avoid having to prescribe many parameters (thickness and vertical permeability of the vadose zone; structure, transmissivity, storage coefficient of aquifers; seepage coefficient describing head loss between river and water table), which are related to physical quantities that are not known in all studied river basins, and for which effective values at the grid scale are difficult to define.

Groundwater transfer being neglected, all water transfers across grid-cells occur in the surface drainage network, and we refer to this process as riverflow routing. The latter is performed in RiTHM at the daily

timestep, under the assumption of pure translation. Thus, the transfer from one cell is completely independent from the transfer from any other cell, and from any possible interaction with the environment (like evaporation, flooding, etc.). Under this assumption, the transfer time t_{adj} between two adjacent cells is defined by

$$t_{\text{adj}} = k \frac{d}{\sqrt{\tan\beta}} \tag{3}$$

where d is the distance and $\tan\beta$ the slope between the two grid-points, and where k is a scaling parameter, including the influence of roughness of the river bed. This formulation can be seen as a simplification of Strickler's formula, the influence of the water stage being neglected. At a larger scale, the river basin is characterized by two basin-wide quantities. L_{abs} is a purely topographical characteristic, equal to the sum of the ratio of distance to slope following the longest path (i.e. the path that maximizes the sum):

$$L_{\text{abs}} = \sum_{\substack{\text{longest}\\ \text{path}}} \frac{d}{\sqrt{\tan\beta}} \tag{4}$$

The concentration time T_c is the only adjustable parameter of the routing module. It defines the time (in days) required to route water along the longest path, and allows us to scale coefficient k in (3):

$$k = T_c / L_{\text{abs}} \tag{5}$$

Because of its high resolution, RiTHM strongly benefits from the efficient transfer algorithm of MODCOU, based on isochronism. For each cell, the transfer time to the outlet is defined as the sum of the t_{adj} when one follows the drainage network from the chosen cell to the outlet. Using these transfer times, one can subdivide the river basin into isochronous zones, which comprise all cells having a transfer time to the outlet within the same day (in the present case of a daily timestep). The corresponding total water volume is then transferred as a whole toward outlet of the basin (or any predefined intermediate gauging station). Figure 4 illustrates this framework for riverflow routing in the case of the Niger river basin. The transfer times to the outlet decrease from dark to light grey, when the distance to the outlet decreases, this effect being modulated by the influence of the slope. The black cells indicate the main streams, characterized by a contributing area larger than 150 000 km^2. One can then recognize: the Niger river, flowing through Koulikouro and Malanville, with its distinctive concavity; the Benoué river, the easternmost and southernmost affluent of the Niger river; Oued Azaouk, which flows southward to Malanville from the northernmost part of the basin, and is an ephemeral stream.

Figure 5 shows the influence of T_c on the mean routed hydrograph at Malanville. This hydrograph was obtained by forcing RiTHM with the 10-year data set of runoff from the LMD GCM (section 2.2). The resulting monthly streamflow at Malanville was averaged over the last nine years only, to reduce the effects of initial conditions the simulations by both the GCM and RiTHM. In this application of RITHM, we did not allow any infiltration in the riverflow module to delay riverflow compared to total runoff (see section 2.5). Therefore, when T_c=0, the hydrograph is equivalent to the spatial average of mean monthly total runoff over the contributing area at Malanville. When T_c increases, peak discharge is delayed and the entire hydrograph is lagged and damped down, with slower floods and recessions. The effective lag between

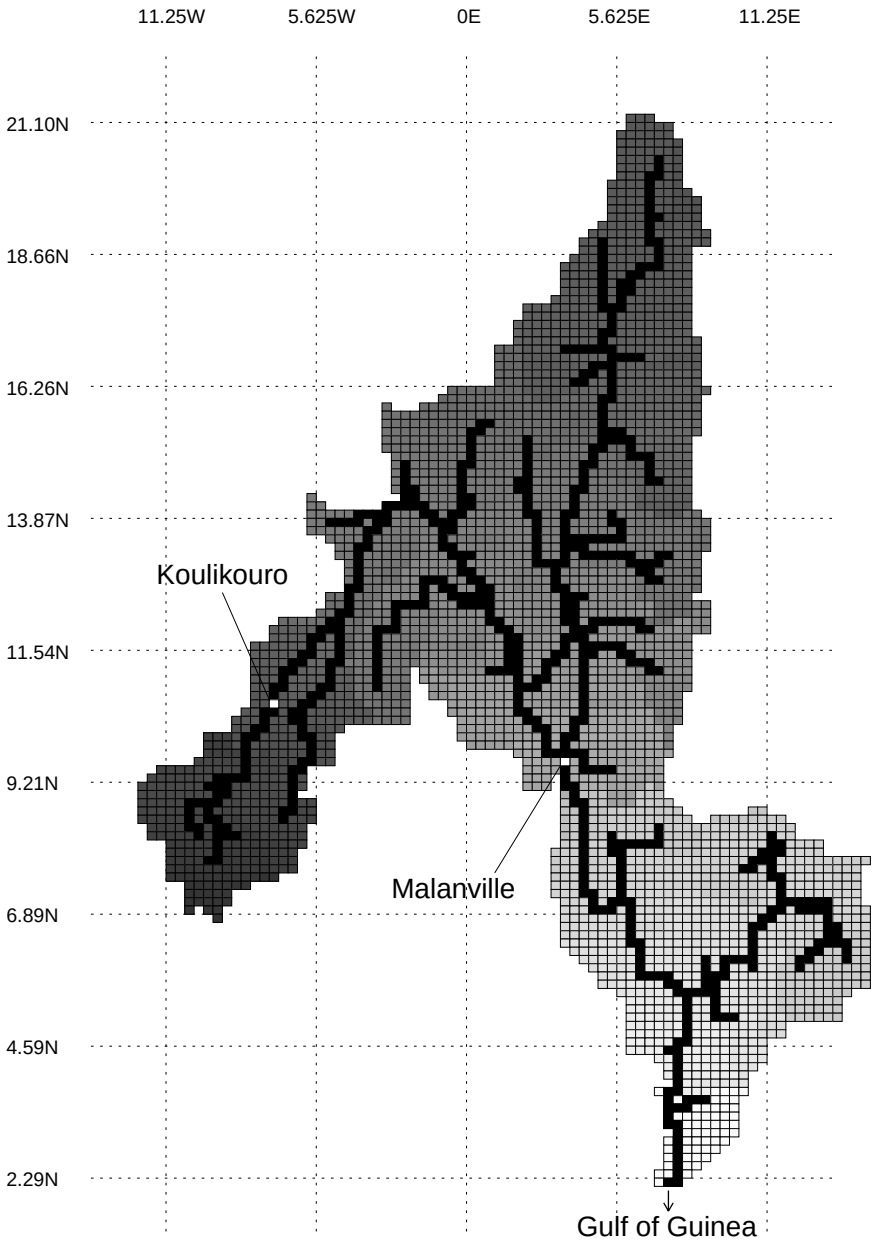

Figure 4: *Spatial discretization of the Niger Basin, and location of two gauging stations: Koulikouro (Mali) and Malanville (Niger). The black cells indicate the main river streams, the transfer times to the outlet decrease from dark to light grey, and the coarse grid is the LMD GCM grid.*

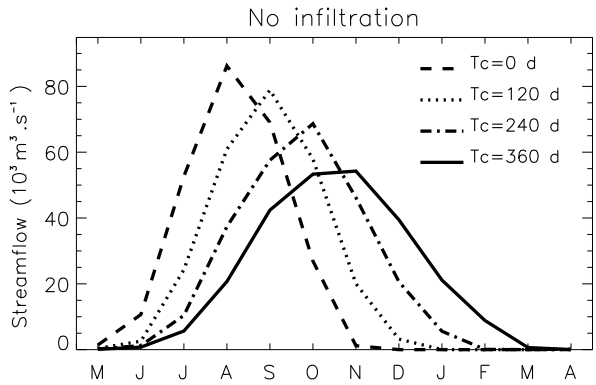

Figure 5: *Influence of the concentration time T_c on the mean annual hydrograph: case of the Niger River at Malanville, with no infiltration allowed. The time axis starts in May.*

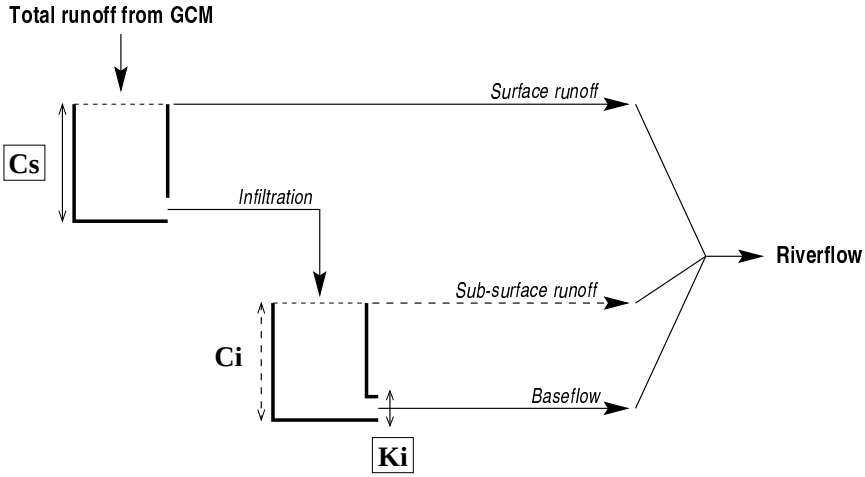

Figure 6: *Transformation of total runoff simulated in the GCM into riverflow, through a series of two reservoirs characterized by three parameters C_s, K_i and C_i (the latter is optional).*

peak runoff and peak discharge is much shorter than the corresponding value of T_c: for instance, the former is about 3 months for the one-year T_c. The reason is that (1) the hydrograph is observed at Malanville and does not correspond to the entire river basin, and (2) rainfall distribution is not homogeneous throughout the basin.

2.5 Riverflow Production

Riverflow production, which chronologically occurs before riverflow routing, is based on a two-reservoir conceptual model at the daily timestep (Figure 6). In every cell of RITHM, the total daily runoff from the GCM is first partitioned between surface runoff and infiltration, using a simple low-pass reservoir, of capacity C_s (in mm.d^{-1}). At every daily timestep, total runoff in excess of C_s comprises surface runoff, which is an instantaneous contribution to riverflow from the cell; the rest, lower or equal to C_s, is entirely transferred to an infiltration reservoir, through which it is delayed before being added to riverflow. This

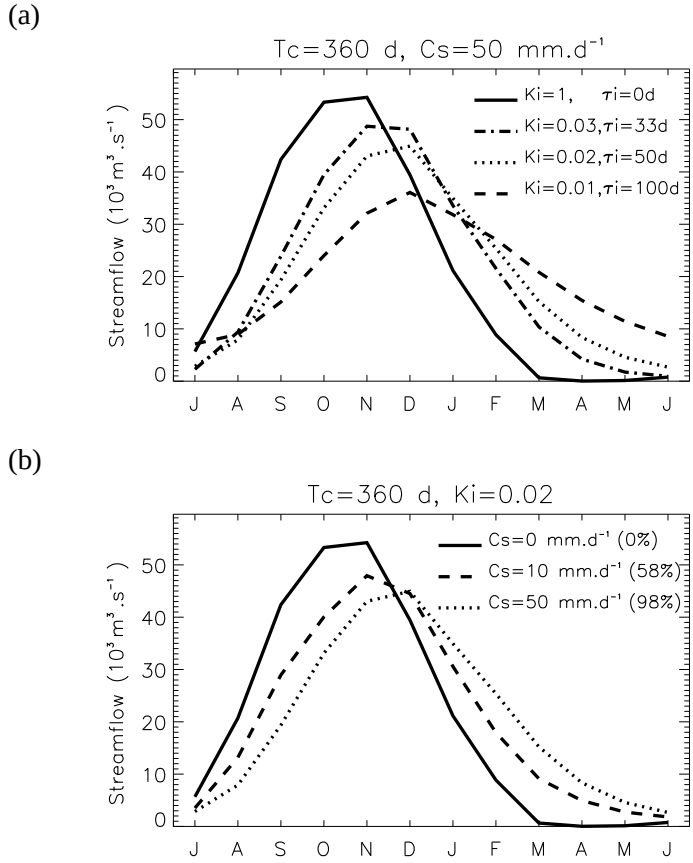

Figure 7: *Influence of the riverflow production parameters on the mean annual hydrograph: (a) recession coefficient K_i (and characteristic timescale τ_i) and (b) capacity of low-pass reservoir C_s. Case of the Niger River at Malanville, with T_c = 360 d. The time axis starts in July.*

reservoir is characterized by a linear recession coefficient K_i (in d^{-1}), so that $Q_i = K_i S_i$ at each timestep. In this equation, Q_i is the resulting delayed infiltration, also called baseflow in RiTHM, and S_i is the volume stored in the reservoir. This volume may be limited by the capacity C_i (in mm). For simplicity, however, this last functionality was not used in the present application, in order to remove one non-linearity.

Figure 7 shows the influence of the two remaining parameters on the mean annual hydrograph of the Niger river at Malanville (with T_c = 360 days). When K_i = 1 d^{-1}, infiltration is not delayed by the infiltration reservoir and the only difference between total runoff from the GCM and streamflow is due to routing (see Figure 5). The same behavior occurs when C_s = 0 mm.d^{-1}, which cancels infiltration.

The parameter K_i can be related to a characteristic timescale τ_i (d), which corresponds to (1) the time required to divide any stored volume by $e = e^1$, and (2) the timelag between runoff and riverflow centroids (Dingman, 1994). When K_i decreases (Figure 7a), this timescale increases, and peak discharge is delayed. This corresponds to slower floods and recessions, and a flatter hydrograph. The three examined values for K_i: 0.01, 0.02, 0.03 d^{-1}, corresponding to characteristic timescales τ_i between 33 and 100 days, are in the range of published values (e.g. Pilgrim and Cordery, 1992; Liston et al., 1994; Hagemann et Dümenil, 1998; Arora and Boer, 1999) for interflow (return flow from infiltration in the soil and vadose

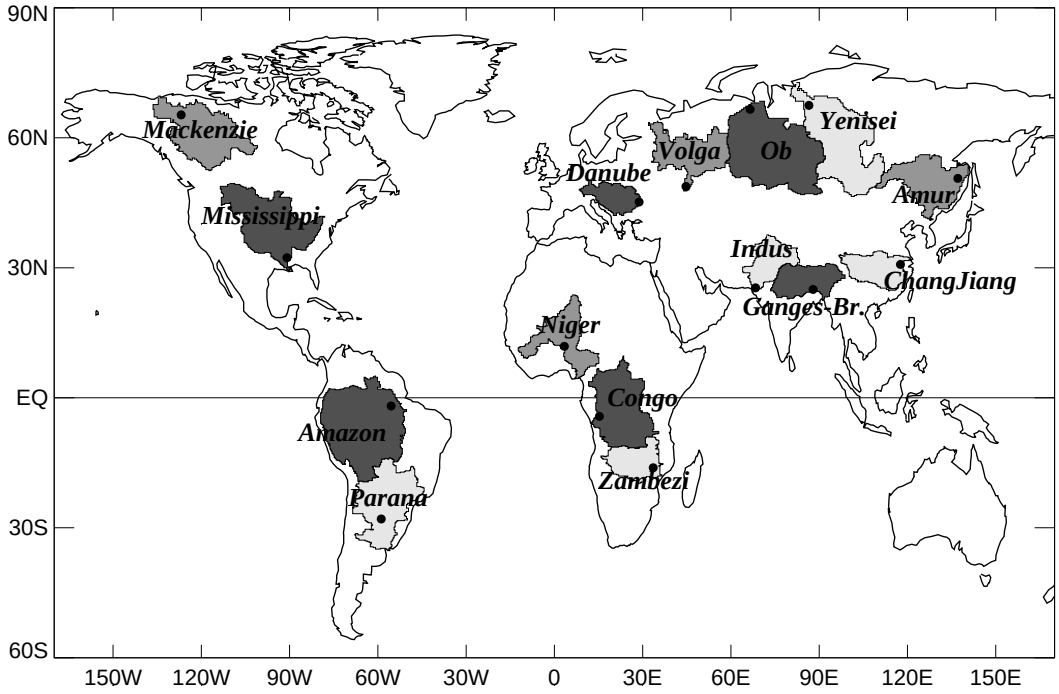

Figure 8: *Selection of 15 river basins and gauging stations (dark dots).*

zone) and baseflow (return flow from groundwater). They tend to be smaller than the K_i values commonly used in MODCOU, that range between 0.1 to 0.02 d^{-1} (Ledoux, 1980; Gille, 1985; Boukerma, 1987). The reason is that the infiltration reservoir of RITHM accounts for the delay caused by infiltration into the soil but also by vertical flow through the vadose zone and by the much slower horizontal groundwater flow, which are both explicitly described in MODCOU. K_i = 0.01 d^{-1}, however, imposes an excessive lag on infiltration in all studied river basins (presented in section 3).

A similar lag and damping down of the hydrograph happens when C_s increases (Figure 7b), because more water is then delayed infiltration. The commonly used values for this parameter ($\leq$ 100 mm.d^{-1}) are in the range of the hydraulic conductivity of soils (e.g. Rawls et al, 1992). Another interesting interpretation of C_s is to relate this parameter to the percentage of total runoff that infiltrates in a given basin over the entire simulation period. This makes it possible to identify the variations of C_s which are significant in regard to the basin hydrology. In the following evaluation of RiTHM, in order to minimize the need for calibration, the value K_i=0.02 d^{-1} was used in all grid-cells and the importance of infiltration delay was adjusted using C_s only.

3 Application to 15 macro-scale river basins

The drainage network was extracted in 152 of the largest river basins around the world. It covers a high fraction of land masses, with the exception of smaller coastal river basins and endorheic basins. Fifteen of the largest river basins, shown in Figure 8, were selected to test RiTHM, based on the availability of

observed streamflow data and the representativity of the hydrometeorology of these basins. In these basins, RiTHM was forced with the 10-year dataset of total runoff simulated by the LMD GCM (Figure 2 and section 2.2). Our primary goal was to evaluate the skills of the association of RiTHM and the GCM to reproduce observed streamflow. Specific questions were: how well is it possible to calibrate RiTHM's two free parameters (T_c and C_s), and what is the quality of the resulting simulated streamflow ?

An important concern in this framework was the strong systematic errors of the LMD GCM on precipitation and total runoff (section 2.2). This prevents the time-accumulated volume of streamflow from being accurate, as well as any good adjustment of simulated streamflow to the observed one. Given that the main difference between streamflow and the spatial accumulation of total runoff is the timelag between these two quantities, it was decided to focus on the correct reproduction of this timelag for the calibration of T_c and C_s . The timelag between peak runoff and peak discharge was emphasized, since the simulation of floods is expected to have a higher impact on the coupled system than that of low flows (related to a smaller freshwater input to oceans).

We considered observed streamflow data from two often redundant sources: the GRDC and the International Satellite Land Surface Climatology Project (ISLSCP; Sellers et al., 1996), which themselves originate for a large part from U.N. Educational, Scientific and Cultural Organization data (UNESCO, 1993). In each basin, we selected the furthest downstream available gauging station (Figure 8), where streamflow integrates runoff from a high fraction of the basin. Additional gauging stations can of course be considered, as illustrated in the case of the Niger river (Figures 4 and 11) Most observed streamflow data were given monthly, with gaps in the time series, and over a time frame that generally had, at best, a few years in common with the 1979-1988 GCM simulation period. As a result, we compared in each basin the inter-annual mean hydrographs (composed of 12 mean monthly values of discharges) obtained from: (1) observed data over the entire available period (climatological means), and (2) simulated discharge at the selected gauging station, over 1980-1988 only (1979 was discarded to reduce the effects of initial conditions on both the GCM and RiTHM simulations). Similarly, precipitation simulated in the LMD GCM over 1980-1988 was compared on average over each river basin to the gauge-corrected climatology of Legates and Willmott (1990).

At this stage, several objective criteria exist to assess the quality of riverflow simulation compared to observation. The efficiency of Nash and Sutcliffe (1970), which derives from linear regression techniques, is one of the most widely used. However, it is not adequate in the present case, where the compared hydrographs are composed of only 12 values and can have very different means. Therefore, the subjective adjustment of the simulated to the observed hydrograph, in terms of timelag especially, was privileged. Yet, this adjustment was evaluated by means of statistical criteria, like Spearman's rank-order correlation coefficient, bias, standard error, or the normalized error defined by Miller et al. (1994) for mean annual cycles at the monthly timestep:

$$\phi = \frac{\sqrt{\sum_1^{12}(X_{\mathrm{sim}} - X_{\mathrm{obs}})^2}}{\sqrt{\sum_1^{12} X_{\mathrm{obs}}^2}}. \tag{6}$$

In this formula, X_{obs} is the observed climatological monthly streamflow near the outlet, and X_{sim} is the

Table 1: *Selected values, in 14 river basins, of C_s (given in mm.d^{-1} and in percent of total runoff that infiltrates over the simulation period) and T_c, given in days, and related to a mean velocity U of riverflow runoff in the basins.*

Rivers	C_s		T_c	U
	(mm.d^{-1})	(%)	(days)	(m.s^{-1})
Amazon	30	92.	105	0.50
Congo	0	0.	120	0.41
ChangJiang	15	68.	105	0.40
Yenisei	10	67.	60	2.78
Mississippi	8	75.	15	2.24
Paraná	40	95.	90	0.54
Ob	5	59.	180	0.48
Ganges-Br.	15	44.	90	0.36
Amur	0	0.	195	0.19
Volga	0	0.	180	0.19
Danube	8	77.	90	0.56
Zambezi	15	76.	120	0.42
Indus	5	36.	30	0.70
Niger	30	90.	360	0.15

mean monthly riverflow simulated at the observation site. This normalized error ϕ can also be used to assess the quality of the precipitation simulated by the GCM. It is zero if the simulated and observed quantities are identical, and it increases (to a value that can markedly exceed 1) when the error increases.

4 Results

4.1 Mean annual cycle of river discharge

It was possible to determine a couple (C_s, T_c) to realistically phase the maximum streamflow in all basins, with the exception of the Mackenzie river basin, where the spatial distribution of the simulated precipitation is highly unrealistic (Ducharne, 1997). It is noteworthy that in most basins, many parameter couples give very similar results, the quality of which cannot be easily discriminated. One of these couples (C_s, T_c) is

given in Table 1 for the remaining 14 basins. The concentration time T_c can be related to a mean velocity U over the basin. In most basins, it falls in the range 0.15-1.00 m.s^{-1} used by many authors for large-scale river velocities (see review by Oki et al., 1999). The only two exceptions are found in the Mississippi and Yenisei river basins, where the calibration of T_c helps to override the incorrect timing of the annual cycle of runoff (see next and section 4.2).

As an example of the type of adjustment that was achieved with parameters from Table 1, Figure 9 compares the mean annual cycle of observed and simulated streamflow, close to the outlet of the Amazon, Ganges and Mississippi. Figure 9 also shows the mean annual cycle of observed and simulated precipitation over these river basins. Streamflow is strongly underestimated for the Amazon; conversely, it is strongly overestimated for the Ganges and the Mississippi. These departures from observed values are in all cases related to differences between climatological and simulated precipitation. In accordance with Figure 2, the latter is underestimated in the first case and overestimated in the last two cases, which include large mountainous areas.

Despite these errors in volume, it was possible in all three cases to phase the simulated and observed streamflow peak. For the Mississippi, however, this phase adjustment is rather artificial, since the simulated precipitation is not well phased with the climatological annual cycle. In the latter, maximum precipitation occurs in June, i.e. two months after maximum observed streamflow, in April. This advance of peak streamflow on peak precipitation is evidence of the importance of spring snowmelt (from the Rocky Mountains in the present case) for runoff production. In the GCM, maximum precipitation is not only higher than in the climatology, but it also occurs earlier (in April, the month of observed peak streamflow). Therefore, spring runoff production related to snowmelt is increased in the GCM by runoff related to high precipitation rates. This explains why peak streamflow is so greatly overestimated in the Mississippi river. This additional runoff, which is produced too early, also explains why the concentration time T_c is so short (15 days, corresponding to a mean velocity U = 2.24 m.s^{-1}). The above examples indicate that the quality of streamflow adjustment is all the better as precipitation is well simulated by the GCM.

The quality of the 14 simulations is summarized in Table 2, where the river basins are ordered following decreasing observed mean streamflow. The statistically significant correlation coefficients between the 12 observed and simulated monthly means of streamflow indicate the good reproduction of the seasonal cycle. The only non-significant correlation coefficient is found in the Congo river, where the extreme overestimation of simulated mean streamflow (bias reaching 150% of mean observed streamflow), combined with a poor spatial distribution of the GCM rainfall (Ducharne, 1997), prevents any meaningful adjustment of simulated streamflow. As a result, we did not attempt to account in this basin for the influence of infiltration on the shape of the hydrograph and the only tuned parameter was T_c (Table 1).

Table 2 also shows that bias, quantifying systematic error, is an important term of total error (bias is in most cases higher or at least as high as standard error). In addition, the sign of this bias is generally identical to the sign of the bias in precipitation. The only exceptions occur in the Paraná, Yenisei, Amur and Volga. In the first basin, the negative annual bias in precipitation is made of underestimation during the dry season (boreal summer) and overestimation during the rainy season (boreal winter); the latter is the cause of

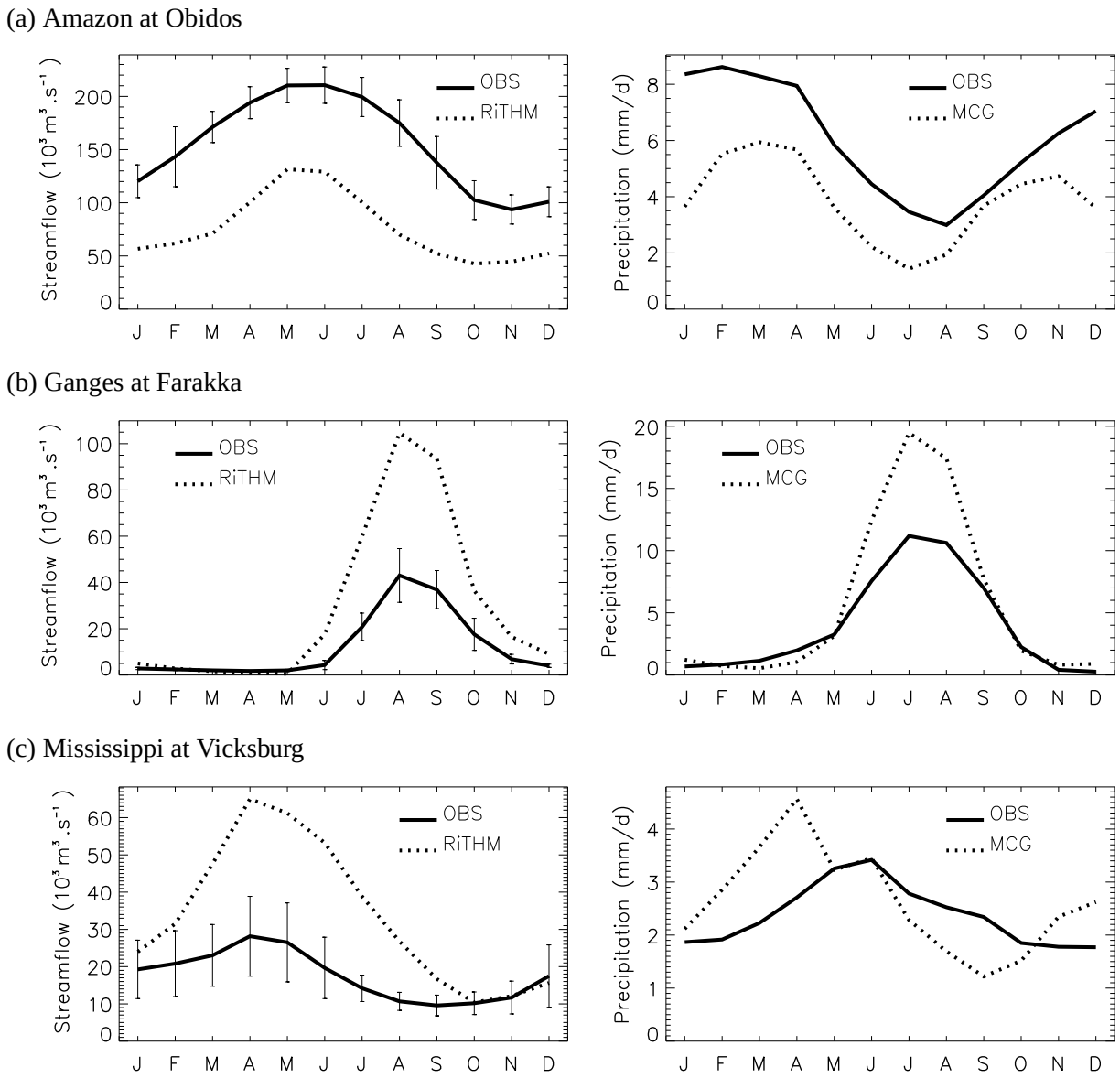

Figure 9: *Comparison of observed and simulated discharge and precipitation over (a) Amazon, (b) Ganges and (c) Mississippi. Observed values are the climatological means described in section 3, from the GRDC for discharge, and from Legates and Willmott (1990) for precipitation. The vertical bars define the standard deviation of monthly observed streamflow over the record period.*

Table 2: *Summary of RiTHM results in 14 river basins (column 1): comparison of observed (column 2) and simulated (column 3) streamflow, in terms of the Spearman's rank-order correlation coefficient (∗/† indicates a significant correlation at the level α=0.05/0.10) between the 12 monthly means (column 4), bias (column 5), standard error (column 6), and the normalized flow error of Miller et al. (1994) (column 7); comparison of observed (column 8) and simulated (column 9) precipitation, in terms of bias (column 10), standard error (column 11), and the normalized precipitation error of Miller et al. (column 12).*

Rivers	Streamflow (10^3 $m^3.s^{-1}$)						Precipitation ($mm.y^{-1}$)				
	OBS	RiTHM	ρ	Bias	σ_{err}	ϕ_Q	OBS	GCM	Bias	σ_{err}	ϕ_P
Amazon	154.9	76.1	0.93*	-78.8	18.7	0.51	2205	1413	-792	420	0.52
Congo	39.5	99.4	0.25	59.9	61.4	2.13	1606	1955	349	475	0.55
ChangJiang	28.9	60.4	0.88*	31.5	9.2	1.03	1207	2166	959	356	0.33
Yenisei	17.8	10.7	0.91*	-7.1	13.8	0.58	423	476	53	200	0.49
Mississippi	17.6	33.6	0.81*	16.0	13.8	1.13	865	960	95	316	0.53
Paraná	16.6	41.4	0.98*	24.8	28.8	2.25	1242	1206	-36	349	0.63
Ob	12.5	6.3	0.76*	-6.2	6.2	0.55	513	367	-146	197	0.47
Ganges-Br.	12.0	29.0	0.99*	17.0	21.8	1.50	1436	2049	613	1092	0.38
Amur	9.7	9.1	0.90*	-0.6	2.6	0.22	576	671	95	422	0.40
Volga	8.1	5.8	0.56†	-2.3	2.1	0.30	659	508	-151	226	0.51
Danube	6.5	12.9	0.96*	6.4	5.5	1.27	884	1072	188	582	0.35
Zambezi	3.3	35.3	0.66*	31.9	24.1	11.57	1050	1730	680	499	0.41
Indus	2.2	14.6	0.80*	12.3	13.0	4.75	451	578	127	222	0.48
Niger	1.1	20.2	0.87*	19.2	14.8	20.31	797	1166	369	298	0.49

streamflow's overestimation and positive bias. The Yenisei, Amur and Volga are high-latitude rivers, where maximum discharge occurs in spring due to snowmelt. Another common point between them (and with the Ob river) is that the LMD GCM markedly underestimates precipitation in summer and overestimates it in winter/spring. The relationship between the biases in precipitation and streamflow depends in each case on the relative magnitude of precipitation's over- and underestimation; in addition, the quality of simulated streamflow is influenced by the representation of snow processes in the LMD GCM, as detailed in section 4.2 for the Yenisei river. This bias analysis confirms that precipitation's systematic error propagates into streamflow's systematic error, as already shown Figure 9.

As stated by Miller et al. (1994), large values of their normalized flow error ϕ_Q are due to a combination of (1) poor source runoff, related to poor GCM precipitation by means of error propagation, and (2) poor simulation of river water transfer. Table 2 shows that ϕ_Q is almost always greater than the normalized precipitation error ϕ_P, which indicates, again, the strong control of precipitation on riverflow. In three rivers (Zambezi, Indus, and Niger), ϕ_Q is much higher than ϕ_P, which indicates that the river water transfer itself is in question. All three rivers, like the Paraná for which $\phi_Q > 3.5\ \phi_P$, flow across very arid subtropical areas. We believe that an additional source of error is related to river transfer in this specific hydroclimatic regime, as explained in section 4.3 in the case of the Niger river.

4.2 A high-latitude case study : the Yenisei basin

The Yenisei river is examined here as a representative example of high-latitude rivers. As such, its peak discharge is strongly controlled by spring snowmelt, as shown in Figure 10 by the advance of observed peak discharge (in June) compared to observed maximum precipitation (in July). As for simulated streamflow, it is underestimated throughout the year, but more markedly so at the time of peak discharge. The underestimation of streamflow in late summer and fall is related to the significant underestimation of precipitation in summer by the GCM. Such a direct relationship between precipitation and streamflow errors does not explain for the underestimation of peak discharge. One reason is that precipitation is not underestimated, but overestimated, in winter and spring, when the flood wave builds up. A more fundamental reason is that the main control on peak discharge is spring snowmelt and not rainfall. The third panel in Figure 10 shows that the GCM accounts for this important contribution of snowmelt to runoff. In April, most of the available water, from either snowmelt or precipitation, infiltrates and brings the soil toward saturation. This produces strong runoff in May, equal to the volume of snowmelt. In contrast, runoff is much weaker during the following months, when snow has disappeared and the only water input is rainfall.

In this high-latitude framework, the underestimation of peak discharge in RiTHM is likely to be related to the underestimation, by the GCM, of runoff originating from snowmelt. One possible reason can be the underestimation of snowfall in the GCM. The maximum of simulated snow depth, spatially averaged over the Yenisei basin, occurs in March, which is realistic compared to the climatology of the US Air Force (Foster and Davy, 1988). This maximum is slightly underestimated (390 mm instead of 415 mm). However, converted to water equivalent using a mean snow density of 300 kg.m^{-3} and spread over the

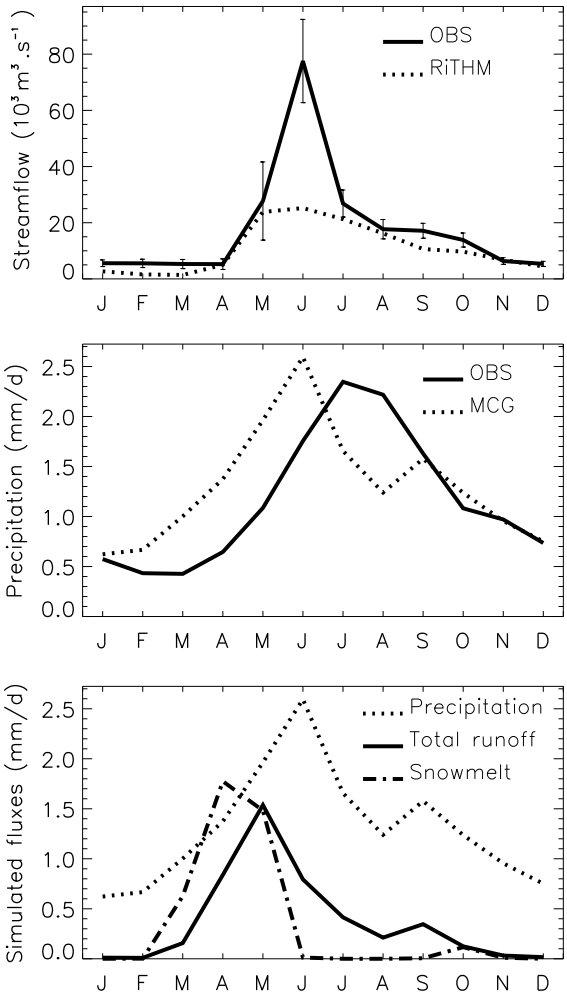

Figure 10: *Comparison of observed and simulated discharge and precipitation in the Yenisei basin at Igarka, and mean annual cycle of simulated water fluxes (precipitation, total runoff, and snowmelt). See Figure 9 for further details.*

two months of melting, this gives a mean snowmelt underestimation of 0.125 mm.d^{-1}, which is negligible compared to the underestimation of runoff and discharge. A more likely reason for runoff underestimation is related to runoff parameterization itself. Overland flow is only produced by a saturation-excess mechanism, with no dependency of runoff on the intensity of water input. Because this intensity is very high at the time of snowmelt, runoff would be increased if this dependency were accounted for (leading to infiltration-excess, or Hortonian, runoff).

Another likely reason for the weakness of runoff production at the time of snowmelt is the absence in the LMD GCM of freezing in the soil. At the latitude range of the Yenisei river basin, such freezing can be permanent (permafrost) and occurs close to the soil surface. This creates an impermeable layer, which strongly limits the effective water-holding capacity of the soil, and therefore enhances surface saturation and overflow runoff production. Neglecting this process is not realistic at such high latitudes, and must explain at least a part of the runoff underestimation observed in the Yenisei basin (as well as in the other studied high-latitude river basins). In addition, the melting of the soil ice, fully or superficially in case of permafrost, can give rise to summer perched water tables. Robock et al. (1995) suggest that the latter are an important source of moisture for summer evapotranspiration in the Siberian plains. The absence of such water tables in the LMD GCM might contribute to the underestimation of high-latitude summer precipitation, owing to the importance of evaporation recycling in these areas in summer (Brubaker et al., 1993).

4.3 A sub-tropical case study : the Niger basin

The behavior of RiTHM is analyzed in the Niger basin to illustrate and understand the important error of simulated streamflow in subtropical rivers. Figure 11 compares the observed and simulated streamflow of the Niger river at two stations, located in Figure 4. Koulikouro is in the upstream part of the basin and Malanville is closer to the outlet, and their respective contributing areas are 120,000 km^2 and 1,000,000 km^2 according to the GRDC. The right panels in Figure 11 compare the climatological and simulated mean annual cycle of precipitation in the above two contributing areas.

At both stations, the general shape of the hydrograph and the timing of maximum and minimum streamflow are well represented by RiTHM. It represents well the one-month timelag between maximum precipitation and streamflow at Koulikouro, and the increase of this timelag at Malanville. However, the simulated streamflow is markedly overestimated. At Koulikouro, this overestimation is strongly related to that of the GCM precipitation in the contributing sub-basin. At Malanville, it is important to notice that the solid curve for streamflow does not represent the observed values, but 10 times the observed values. This means that the actual overestimation of the simulated streamflow is extreme, as can also be seen from the striking value of 1745% for the bias of streamflow relatively to mean observed streamflow (Table 2). In particular, it cannot be explained by the overestimation of precipitation only, even if the latter is somewhat larger at Malanville than at Koulikouro.

The shape of the hydrograph is another important difference between simulation and observation. At the period of highest discharge at Malanville, which is also the dry season (see the annual cycle of

(a) Niger at Koulikouro

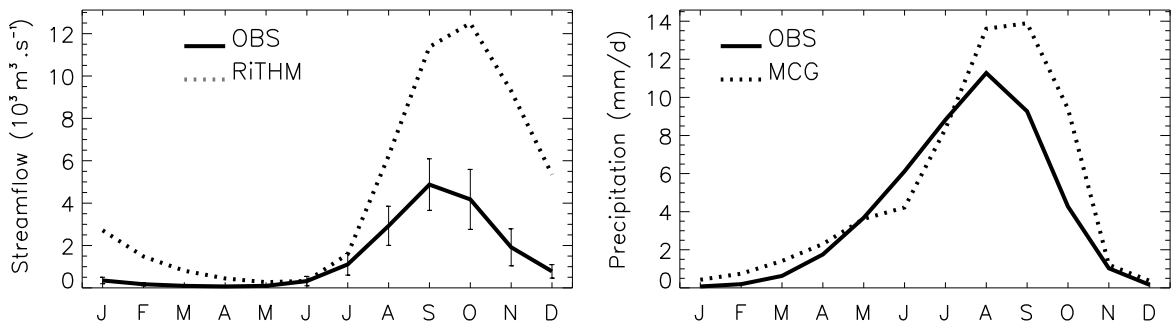

(b) Niger at Malanville

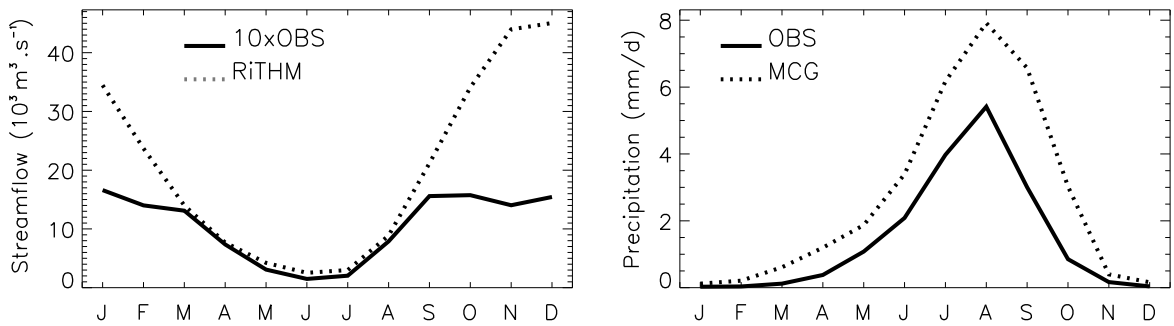

Figure 11: *Niger basin: comparison of observed and simulated discharge at two stations: (a) Koulikouro, (b) Malanville, and of precipitation in the respective contributive areas. For streamflow at Malanville, the solid curve gives 10 times the observed streamflow. See Figure 9 for further details.*

precipitation), the observed hydrograph is very flat, as if low-pass filtered compared to the shape of the simulated hydrograph. Our interpretation is that the real peak streamflow has been damped at Malanville by evaporative processes that are not accounted for, in either RiTHM or the GCM. These processes include direct evaporation from the river and evaporation from the connected areas, either natural or agricultural, in which case the connection to the river is usually driven by irrigation. The impact of this damping is especially noticeable in the Niger river because of the length of the main stream; when the flood wave (produced during the rainy season centered in August) arrives at Malanville, the dry season has started and this maximizes evaporation.

4.4 Towards an objective determination of the concentration time

In the 14 river basins of Table 1, the most effective parameter was the concentration time T_c, which controls the speed of large-scale transfers in the drainage network. The purpose of this section is to help the determination of this important parameter.

In small-scale river basins, many empirical relationships exist between the basin concentration time and geomorphological quantities. The most commonly used are the basin area A, the length of the longest stream L, and the mean overland slope S. A particular example is the formulation of the transfer time between two adjacent cells in RiTHM (equation 3). Many empirical laws also relate T_c to the volume of water transfered through the basin. This comes from Saint-Venant's equations, which describe the conservation of mass and momentum in a given river stretch. They relate flow velocity to the water level in the stretch, itself related to a water volume owing to the constant geometry of the stretch over time. Askew (1970) proposes the following law for the concentration time of floods (time lag between the centroids of excess precipitation and flood discharge), in basins that are smaller than 100 km^2:

$$T_f = 0.0366\, L^{0.80}\, S^{-0.33}\, {Q_f}^{-0.23} \tag{7}$$

In this law, Q_f is the mean discharge during floods in m^3.s^{-1}, L is in km, S is dimensionless, and T_f is in days. In another example, proposed by Vörösmarty et al. (1989) for grid-cells of length L=55 km, the mean annual time lag of a cell is proportional to its length L, a sinuosity factor, and the inverse of mean annual discharge at the outlet of the cell.

We devised a similar approach, under which we related T_c (in days) to a geomorphological quantity, the absolute length $L_{\rm abs}$ (defined in section 2.4 as the sum following the longest path of the ratio of distance to square root of slope, unit = km), and to the mean annual simulated streamflow at the furthest downstream station $Q_{\rm am}$ (in m^3.s^{-1}). Infiltration was canceled here to determine T_c, so that the latter could account for the total lag. Figure 12 shows the relationship between T_c and the ratio $L_{\rm abs}/Q_{\rm am}$. The corresponding linear regression gives:

$$T_c = 32 + 56\, L_{\rm abs}/Q_{\rm am}, \tag{8}$$

with a significant linear correlation coefficient ρ = 0.80. The latter can be increased if one optimizes the

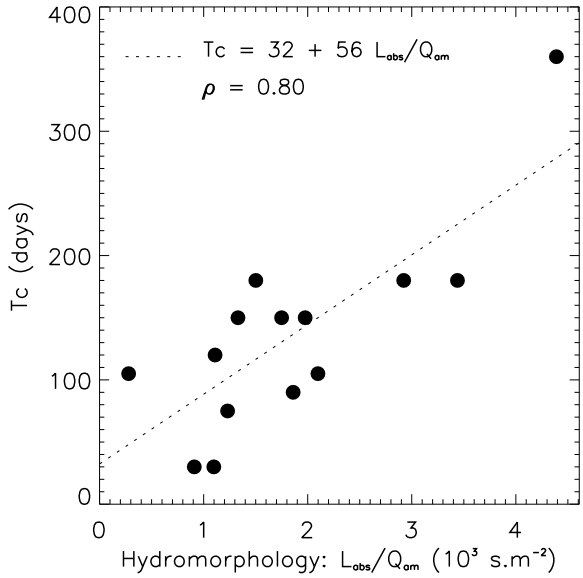

Figure 12: *Correlation between the calibrated concentration time T_c (with C_s = 0 mm.day^{-1}) and a characteristic of both geomorphology and the hydrologic regime: $L_{\mathrm{abs}}/Q_{\mathrm{am}}$. See text for details, including units.*

exponents of L_{abs} and Q_{am}. This leads to the following law:

$$T_c = 65 + 0.51\, {L_{\mathrm{abs}}}^{1.71} {Q_{\mathrm{am}}}^{-1.33}, \tag{9}$$

and the linear correlation coefficient ρ = 0.89.

If these laws display strong analogies with the ones proposed for small-scale basins (length in numerator, slope and mean annual downstream discharge Q_{am} in denominator), the parameters themselves are highly different. For instance, using equation 7 for the 14 studied basins (replacing $L^{0.80}\, S^{-0.33}$ with ${L_{\mathrm{abs}}}^{0.80}$) gives concentration times that range in [7,35] days, whereas the calibrated values (with C_s = 0 mm.day^{-1}) range in [30,360] days. The values predicted by equations 8 and 9 fall much closer to this range, as shown in Table 3. We postulate that the differences in parameters correspond to a scale effect. It can be related to many reasons, including the heterogeneity of rainfall and soil properties in large-scale basins (whereas a small-scale basin can be assumed to have more homogeneous properties), the influence of groundwater flow on flow velocity, and the different hydraulics in large and small streams.

The main motivation behind the proposed two laws was to assist the calibration of T_c. One interpretation of the correlation coefficient is that equation 9 (respectively 8) explains ρ^2 = 79% (respectively 64%) of the total variance of T_c among the 14 river basins. This permits us to use these equations to restrict the range of possible values for T_c, around the values predicted using L_{abs} and Q_{am}, which can be calculated by RiTHM with any parameter set (for example C_s = 0 mm.day^{-1} and T_c = 1 day) because this model conserves water. A subjective adjustment of T_c is still required, because of the unexplained variance and the rather high standard error of the estimations (Table 3). One must also keep in mind that equations 9 and 8 are empirical, based on 14 river basins only, and likely to be inappropriate in many cases. In addition,

Table 3: *Summary of the performance of equations 8 and 9 in terms of predicted T_c.*

	Predicted T_c		
	Range (in d)	Standard error (in d)	Standard error (in % of average calibrated T_c)
Equation 8	[48,280]	47	34%
Equation 9	[70,345]	36	27%

infiltration needs to be accounted for in the total lag, and this shall reduce T_c which accounts in RiTHM for the sole lag caused by transfer in surface drainage network. Last but not least, an important limitation of equations 9 and 8 lies in their dependence on Q_{am}, which is not constant over the climatic record. Since this dependence is based on physical considerations (the intrinsic relationship between velocity and discharge), the concentration time of a basin, even if carefully calibrated using existing data, is likely to require a change for studies of paleo-climates or future climate change.

5 Discussion and conclusions

We have described a new runoff routing model (RRM) for use in GCMs. This model, RiTHM, which can be seen as an adaptation to the macro-scale of the hydrological model MODCOU (Ledoux et al., 1989), has two main features compared to RRMs previously used in GCMs (e.g. Miller et al., 1994; Liston et al., 1994; Hagemann and Dümenil, 1998; Arora and Boer, 1999). The first is a high spatial resolution ($\simeq 25\times 25$ km^2), allowing a precise delineation of macro-scale river basins and the capture of sharp topographic contrasts. The second original feature, related to the first one by means of computational cost reduction, is the simplicity of its routing algorithm. The lateral transfer across grid-cells is performed in the surface drainage network only, under the assumption of pure translation. This implies that the transfer from one cell is independent of the transfer from any other cell, and of any possible interaction with the environment (like re-evaporation, flooding, etc.). Therefore, it only depends on topography and a basin-wide parameter, the concentration time T_c. Groundwater flow (in the soil, unsaturated zone and aquifers) is only considered within the cells, under the assumption that there is at least one stream in every 625 km^2 cells to insure the local discharge of groundwater to the river. Therefore, its contribution to total lag is simply described by a linear infiltration reservoir.

RiTHM has been successfully applied to 14 of the world's largest river basins, where it was forced, at the daily timestep, by 10 years of total runoff simulated by the LMD GCM. In this GCM framework, an important result, although not new (e.g. Miller et al., 1994; Arora and Boer, 1999), is that the quality of simulated streamflow is strongly limited by the quality of GCM simulated precipitation. Any error in this term, with respect to total amount, seasonal variations or spatial distribution, affects total runoff (RITHM's

input), and therefore induces errors in simulated streamflow.

As a result, the application presented in this paper cannot be seen as a proper validation of the model RiTHM. The latter is required, however, if one wants to use this RRM as a validation tool for the GCM's LSM, or as an interactive component in a coupled GCM. This would require that RiTHM was forced with better fields of total runoff than those simulated by GCMs. One could use composite runoff fields such as those derived by Fekete et al. (2000), at the $0.5° \times 0.5°$ resolution and daily timestep, from observed river discharge and a simple water balance model. An alternative approach is to force a state-of-the-art LSM (like SECHIBA in the present study) with observational near-surface meteorological data. As an example, the ISLSCP Initiative I dataset (Sellers et al., 1996), at the $1° \times 1°$ resolution and 6-hourly timestep, has already been used in the Global Soil Wetness Project (Dirmeyer et al., 1999) to assess runoff from different LSMs using a RRM (Oki et al., 1999).

Despite important errors in streamflow volume related to GCM precipitation inaccuracies, this work has proved possible to realistically reproduce the seasonal variations of streamflow, and, more specifically, the timing of its maximum. This was achieved through the tuning of a minimum number of parameters. We found a uniform recession coefficient K_i = 0.02 d^{-1} to be adequate in all studied basins, and the only tuned parameters were the concentration time and the infiltration capacity C_s, which was chosen as uniform in each basin. The simplification of uniform K_i and C_s has appeared more rigorous than a distributed assignment of these parameters, given the first-order error source from simulated precipitation. Nevertheless, it seems possible, in the future, to relate C_s (and its spatial variations) to physical characteristics of the surface, like hydraulic conductivity, but also vegetation, slope, and any factor likely to modify infiltration towards both soil and aquifers. As for T_c, which is the most effective parameter for fitting the simulated hydrograph, it may be defined *a priori*, using the relationship discussed in section 4.4. This concentration time is the sum of transfer times between adjacent cells following the longest path to the outlet. Note that there exist other formulations of the elementary transfer times than the simple one used in this study (equation 3). An example, proposed by Golaz (1999), is

$$t_{\mathrm{adj}} = k \, \frac{d}{\sqrt{\tan\beta}} \, \frac{1}{{A_{\mathrm{sup}}}^{\alpha}} \quad , \tag{10}$$

where A_{sup} is the upstream contributing area, and α is positive, with values between 0.25 and 1. The last factor represents the fact that a higher contributing area, under unchanged conditions of input runoff and topography, corresponds to a higher discharge, therefore to a higher flow velocity.

The present study has also pointed out an important external error source in addition to GCM precipitation inaccuracies, with possible higher impacts than the formulation of RiTHM itself or the simple parameter assignment. It stems from the inaccurate description of some hydrological processes, such as snow and soil freezing processes at high latitudes, or direct evaporation from the river bed (and hydraulically connected areas) in the subtropics. Beside their effects on hydrographs (section 4.2 and 4.3), these processes are likely to have an impact on climate, either through discharge itself (as illustrated in introduction), or by changing the land/atmosphere fluxes. Freezing modifies the energy budget of soil, leading to higher soil and surface temperatures, which may interact with snow melting and evapotranspiration (e.g.

Stieglitz et al., in press). Evaporation from the rivers or connected wetlands, which occurs at the potential rate, locally decreases surface temperature. The resulting temperature contrasts, as well as the increase in atmospheric moisture, are likely to affect regional precipitation, in terms of both spatial structure and temporal variability.

The above processes must therefore be accounted for interactively in the simulated system, i.e. at the GCM level. Soil freezing and snow processes, as well as infiltration-excess runoff (section 4.2), can be included in the LSM (e.g. Koster et al., 2000; Stieglitz et al., in press). In contrast, the modeling of evaporation from the river streams, the flood plains (very important in the Amazon basin, Vörösmarty et al., 1989), or from any other hydraulic annex, requires a real coupling of the GCM and the RRM. An added-value of RiTHM for such a coupling is to descend from the hydrological model MODCOU. It would therefore be straightforward to reintroduce the physically-based description of groundwater processes from the latter model. This would make it possible to simulate the interactions between groundwater and climate, which can be important with respect to long-term climate variations.

Acknowledgments

Most observed discharge data were provided by The Global Runoff Data Centre, D - 56002 Koblenz, Germany. The GCM simulation used in this study was performed using the computational facilities of the Institut du Développement et des Ressources en Informatique Scientifique (Centre National de la recherche Scientifique).

References

Ambroise, B., Perrin, J. L., and Reutenauer, D., 1995. Multicriterion validation of a semidistributed conceptual model of the water cycle in the Fecht catchment. Water Resour. Res. 31(6), 1467–1481.

Arora, V. and Boer, G., 1999. A variable velocity flow routing algorithm for GCMs. J. Geophys. Res. 104(D24), 30965–30979.

Askew, A. J., 1970. Derivation of formulae for variable lag time. J. Hydrol. 10, 225–242.

Avissar, R. and Pielke, R., 1989. A parametrization of heterogeneous land surfaces for atmospheric numerical models and its impact on regional meteorology. Mon. Weather Rev. 117, 2113–2136.

Boukerma, B., 1987. Modelling of surface and groudwater flow in the South-West of France using a water budget approach. Ph.D. thesis, Ecole Nationale Supérieure des Mines de Paris, Fontainebleau, France (in French).

Brubaker, K. L., Entekhabi, D., and Eagleson, P. S., 1993. Estimation of continental precipitation recycling. J. Clim. 6, 1077–1089.

Campos, E., Lentini, C., Miller, J., and Piola, A., 1999. Interannual variability of the sea surface temperature in the South Brazil Bight. Geophys. Res. Letters. 26, 2061–2064.

Cavazzi, C., 1995. Use of a digital elevation model to help distributed hydrological modelling. Master thesis, Université Paris 6, France (in French).

Choisnel, E. M., Jourdain, S. V., and Jacquart, C. J., 1995. Climatological evaluation of some fluxes of the surface energy and soil water balances over France. Annales Geophysicae. 13, 666–674.

Coe, M. T., 1998. A linked global model of terrestrial hydrologic processes: Simulation of modern rivers, lakes, and wetlands. J. Geophys. Res. 103(D8), 8885–8899.

Coe, M. T., 2000. Modeling terrestrial hydrological systems at the continental scale: Testing the accuracy of an atmospheric GCM. J. Clim. 13, 686–704.

Dingman, S., 1994. Physical Hydrology, 575 pp. Prentice Hall, Upper Saddle River, New Jersey.

Dirmeyer, P., Dolman, A., and Sato, N., 1999. The Global Soil Wetness Project: A pilot project for global land surface modeling and validation. Bull. of the Am. Met. Soc. 80, 851–878.

Ducharne, A., 1997. The water cycle: modelling continental hydrology and studying its interactions with climate. Ph.D. thesis, Université Paris 6 (in French).

Ducharne, A. and Laval, K., 2000. Influence of the realistic description of soil water-holding capacity on the global water cycle in a GCM. J. Clim. 13, 4393–4413.

Ducharne, A., Laval, K., and Polcher, J., 1998. Sensitivity of the hydrological cycle to the parametrization of soil hydrology in a GCM. Clim. Dyn. 14, 307–327.

Ducoudré, N., Laval, K., and Perrier, A., 1993. SECHIBA, a new set of parametrizations of the hydrologic exchanges at the land/atmosphere interface within the LMD atmospheric general circulation model. J. Clim. 6(2), 248–273.

Dümenil, L. and Todini, E., 1992. A rainfall-runoff scheme for use in the Hamburg climate model. In: O'Kane, J. (Ed), Advances in theoretical hydrology, A tribute to James Dooge. European Geophysical Society Series in Hydrological Sciences. Volume 1, pp. 129–157. Elsevier, Amsterdam.

Fekete, B. M., Vörösmarty, C. J., and Grabs, W., 2000. Global, composite runoff fields based on observed river and simulated water balances. UNH/GRDC Composite Runoff Fields V 1.0 CD-Rom. Available from BAHC International Project Office (email : bahc@pik-potsdam.de), or at http://www.grdc.sr.unh.edu/.

Foster, D. J. and Davy, R., 1988. Global snow depth climatology. Technical Report USAF-ETAC/TN-88/006, US Air Force Environmental Technical Application Center, Scott Air Force base, Illinois. Available from the National Climatic Data Center, Ashville, NC 28801.

Gates, W. L., 1992. AMIP, the atmospheric model intercomparison project. Bull. of the Am. Met. Soc. 73, 1962–1970.

Gille, E., 1985. Hydrological study of the Meuse and Moselle river basins. Ph.D. thesis, Ecole Nationale Supérieure des Mines de Paris, Fontainebleau, France (in French).

Golaz, C., 1999. Regional-scale hydrological modelling of the Rhône river basin. Comparison of two methods for water budget computations and sensitivity to a perturbation of climatic forcing. Ph.D. thesis, Ecole Nationale Supérieure des Mines de Paris, Fontainebleau, France (in French).

Gomez, E., Ledoux, E., and Mary, B., 1999. The approach for modelling water and nitrogen production and transfer in the Seine river basin; structure of the hydrological model. Technical report of the Programme PIREN-Seine, Paris, France. pp. 1–13 (in French).

Habets, F., Etchevers, P., Golaz, C., Leblois, E., Ledoux, E., Martin, E., Noilhan, J., and Ottlé, C., 1999. Simulation of the water budget and the river flows of the Rhone basin. J. Geophys. Res. 104(D24), 31145–31172.

Hagemann, S. and Dümenil, L., 1998. A parametrization of the lateral waterflow for the global scale. Clim. Dyn. 14, 17–31.

Koster, R. D. and Suarez, M. J., 1992. Modeling the land surface boundary in climate models as a composite of independants vegetation stands. J. Geophys. Res. 97(D3), 2697–2715.

Koster, R. D., Suarez, M., Ducharne, A., Stieglitz, M., and Kumar, P. (in press). A catchment-based approach to modeling land surface processes in a GCM - Part 1: Model structure. J. Geophys. Res. 105 (D20), 24809–24822.

Le Treut, H. and Li, Z.-X., 1991. Sensitivity of an atmospheric general circulation model to prescribed SST changes: feedback effects associated with the simulation of cloud optical properties. Clim. Dyn. 5, 175–187.

Leblois, E. and Sauquet, E., 2000. Grid elevation models in hydrology - Part 1: Principles and litterature review; Part 2: HydroDem user's manual. Technical note, Cemagref, Lyon, France. 80 pp.

Ledoux, E., 1980. Coupled modelling of surface and groudwater flow in a watershed. Ph.D. thesis, Ecole Nationale Supérieure des Mines de Paris and Université Paris 6, Fontainebleau, France (in French).

Ledoux, E., Girard, G., de Marsily, G., Villeneuve, J.-P., and Deschenes, J. , 1989. Spatially distributed modeling : Conceptual approach, coupling surface water and groundwater. In: Morel-Seytoux, H. J. (Ed), Unsaturated Flow in Hydrologic modeling - Theory and Practice. Volume 275 of NATO ASI Series C, pp. 435–454. Kluwer Academic, Norwell, Mass.

Legates, D. R. and Willmott, C. J., 1990. Mean seasonal and spatial variability in gauge-corrected, global precipitation. International Journal of Climatology. 10, 111–127.

Liang, X., Lettenmaier, D., Wood, E., and Burges, S., 1994. A simple hydrologically based model of land surface water and energy fluxes for general circulation models. J. Geophys. Res. 99(D7), 14415–14428.

Liston, G. E., Sud, C., and Wood, E. F., 1994. Evaluating GCM land surface hydrology parameterizations by computing river discharges using a runoff routing model : application to the Mississipi basin. J. Appl. Meteorol. 33, 394–405.

Maidment, D. R., 1996. GIS and hydrologic modeling : an assessment of progress. Presented at the Third International Conference on GIS and Environmental Modeling, January 22-26, 1996, Santa Fe, New Mexico, USA. Available at http://www.ce.utexas.edu/prof/maidment/.

Miller, J. R., Russel, G. L., and Caliri, G., 1994. Continental-scale river flow in climate models. J. Clim. 7, 914–928.

Murtugudde, R., 1998. The role of river discharges in the interannual variability of the atlantic ocean between 1958-1998. Invited presentation at the TAO Implementation Panel Meeting. (Abidjan, Ivory Coast, November, 1998).

Mysak, L. A., Manak, D. K., and Marsden, R. F., 1990. Sea-ice anomalies observed in the greenland and labrador seas during 1901-1984 and relation to an interdecadal Artic climate cycle. Clim. Dyn. 5, 111–133.

Nash, J. E., 1959. Systematic determination of unit hydrograph parameters. J. Geophys. Res. 61(1).

Nash, J. E. and Sutcliffe, J. V., 1970. River flow forecasting through conceptual models, Part I : a discussion of principles. J. Hydrol. 10, 282–290.

Oki, T., Nishimura, T., and Dirmeyer, P., 1999. Validating land surface models by runoff in major river basins of the globe using Total Runoff Integrating Pathways (TRIP). J. Meteor. Soc. Japan. 77, 235–255.

Oki, T. and Sud, Y. C., 1998. Design of Total Runoff Integrating Pathways (TRIP) A global river channel network Earth Interactions, 2.

Pilgrim, D. H. and Cordery, I., 1992. Flood runoff. In: Maidment, D. R. (Ed), Handbook of Hydrology. McGraw-Hill, Inc, New-York.

NGDC, 1988. Digital relief of the surface of the Earth (ETOPO5). Data announcement 88-mgg-02, NOAA, National Geophysical Data Center, Boulder, Colorado.

Rawls, W. J., Ahuja, L. R., Brabensiek, D. L., and Shirmohammadi, A., 1992. Infiltration and soil water movement. In: Maidment, D. R. (Ed), Handbook of Hydrology. McGraw-Hill, Inc, New-York.

Renssen, H. and Knoop, J., 2000. A global river routing network for use in hydrological modeling. J. Hydrol. 230, 230–243.

Robock, A., Vinnikov, K., Schlosser, C., Speranskaya, N., and Xue, Y., 1995. Use of midlatitude soil moisture and meteorological observations to validate soil moisture simulations with biosphere and bucket models. J. Clim. 8, 1–35.

Rowntree, P. R. and Lean, J., 1994. Validation of hydrological schemes for climate models against catchment data. J. Hydrol. 155, 301–323.

Sadourny, R. and Laval, K., 1984. January and July performance of the LMD general circulation model. In: Berger, A. L. and Nicolis, C. (Ed), New perspectives in climate modelling, pp. 173–197. Elsevier, Amsterdam.

Sausen, R., Schubert, S., and Dümenil, L., 1993. A model of the river-runoff for use in coupled atmopshere-ocean models. J. Hydrol. 155, 337–352.

Sellers, P., Meeson, B. W., Closs, J., Collatz, J., Corprew, F., Dazlich, D., Hall, F. G., Kerr, Y., Koster, R., Los, S., Mitchell, K., McManus, J., Myers, D., Sun, K. J., and Try, P., 1996. The ISLSCP Inititative I global data sets: surface boundary conditions and atmospheric forcings for land-atmosphere studies. Bull. Am. Met. Soc. 77, 1987–2006.

Stieglitz, M., Ducharne, A., Koster, R., and Suarez, M., in press. The impact of detailed snow physics on the simulation of snow cover and subsurface thermodynamics at continental scales. Journal of Hydrometeorology.

UNESCO, 1993. Discharge of selected rivers of the world. vol. 2. part 2. mean monthly and extreme discharges (1965-1984). Technical report, UNESCO Press, Paris. 288 pp.

Vörösmarty, C. J., Moore, B., Grace, A. L., Gildea, M. P., Melillo, J. M., Peterson, B. J., Rastetter, E. B., and Steudler, P. A., 1989. Continental scale models of water balance and fluvial transport : an application to South America. Global Biogeochemical Cycles. 3(3), 241–265.

Weller, R., 1998. The hydrological cycle linking the ocean and atmosphere to land. Invited presentation at the AGU Fall Meeting 1998 (San Francisco, USA). EOS. 79(45), Supplement, p. F13.

Wood, E., Lettenmaier, D., and Zartarian, V., 1992. A land-surface hydrology parameterization with subgrid variability for general circulation models. J. Geophys. Res. 97(D3), 2717–2728.

Déjà paru :

7 : Juin 1998 Marina Lévy, Laurent Mémery and Gurvan Madec, *Combined Effects of Mesoscale Processes and Atmospheric High-Frequency Variability on the Spring Bloom in the MEDOC Area*

8 : Septembre 1998 Carine Laurent, Hervé Le Treut, Zhao-Xin Li, Laurent Fairhead and Jean-Louis Dufresne, *The influence of resolution in simulating inter-annual and inter-decadal variability in a coupled ocean-atmosphere GCM, with emphasis over the North Atlantic.*

9 : Octobre 1998 Francis Codron, Augustin Vintzileos and Robert Sadourny, *An Improved Interpolation Scheme between an Atmospheric Model and Underlying Surface Grids near Orography and Ocean Boundaries.*

10 : Novembre 1998 Z.X. Li and A.F. Carril, *Transient properties of atmospheric circulation in two reanalysis datasets.*

11 : Décembre 1998 Gurvan Madec, Pascale Delecluse, Maurice Imbard and Claire Lévy, *OPA8.1 ocean general circulation model reference manual.*

12 : Janvier 1999 Marc Guyon, Gurvan Madec, François-Xavier Roux, Christophe Herbaut, Maurice Imbard, and Philippe Fraunie, *Domain Decomposition Method as a Nutshell for Massively Parallel Ocean Modelling with the OPA Model .*

13 : Février 1999 Eric Guilyardi, Gurvan Madec, and Laurent Terray, *he Role of Lateral Ocean Physics in the Upper Ocean Thermal Balance of a Coupled Ocean-Atmosphere GCM*

14 : Mars 1999 D. Hauglustaine, *Impact of Biomass Burning and Lightning Emissions on the Distribution of Tropospheric Ozone and its Precursors in the Tropics*

15 : Décembre 1999 L. Menut, R. Vautard, C. Honnoré, and M. Beekmann, *Sensitivity of Photochemical Pollution using the Adjoint of a Simplified Chemistry-Transport Model*

16 : Janvier 2000 J.-Ph. Boulanger, *The Trident Pacific model. Part 1: The oceanic dynamical model and observations during the TOPEX/POSEIDON period*

17 : Janvier 2000 J.-Ph. Boulanger and Christophe Menkes, *The Trident Pacific model Part 2: The thermodynamical model and the role of long equatorial wave reflection during the TOPEX/POSEIDON period*

18 : Octobre 2000 H. Le Treut and B. McAvaney, *A model intercomparison of equilibrium climate change in response to CO_2 doubling*

19 : Octobre 2000 Pierre Friedlingstein, Laurent Bopp, Philippe Ciais, Jean-Louis Dufresne, Laurent Fairhead, Hervé LeTreut, Patrick Monfray, and James Orr, *Positive feedback of the carbon cycle on future climate change*

20 : Février 2001 Agnès Ducharne, Catherine Golaz, Etienne Leblois, Katia Laval, Emmanuel Ledoux, and Ghislain de Marsily, *RiTHM (River Transfer Hydrological Model) : a Runoff Routing Scheme for GCMs*

Plus de détails sont disponibles sur Internet :
http://www.ipsl.jussieu.fr/modelisation/liste-notes.html.